

Direct observation of damage clustering in irradiated DNA with atomic force microscopy

Xu Xu¹, Toshiaki Nakano¹, Masataka Tsuda¹, Ryota Kanamoto¹, Ryoichi Hirayama², Akiko Uzawa² and Hiroshi Ide^{1,*}

¹Department of Mathematical and Life Sciences, Graduate School of Science, Hiroshima University, Higashi-Hiroshima 739-8526, Japan and ²Department of Charged Particle Therapy Research, National Institute of Radiological Sciences, Quantum Medical Science Directorate, National Institutes for Quantum and Radiological Science and Technology, 4-9-1 Anagawa, Inage-ku, Chiba-shi, Chiba 263-8555, Japan

Received May 24, 2019; Revised November 23, 2019; Editorial Decision November 27, 2019; Accepted November 29, 2019

ABSTRACT

Ionizing radiation produces clustered DNA damage that contains two or more lesions in 10–20 bp. It is believed that the complexity of clustered damage (i.e., the number of lesions per damage site) is related to the biological severity of ionizing radiation. However, only simple clustered damage containing two vicinal lesions has been demonstrated experimentally. Here we developed a novel method to analyze the complexity of clustered DNA damage. Plasmid DNA was irradiated with densely and sparsely ionizing Fe-ion beams and X-rays, respectively. Then, the resulting DNA lesions were labeled with biotin/streptavidin and observed with atomic force microscopy. Fe-ion beams produced complex clustered damage containing 2–4 lesions. Furthermore, they generated two or three clustered damage sites in a single plasmid molecule that resulted from the hit of a single track of Fe-ion beams. Conversely, X-rays produced relatively simple clustered damage. The present results provide the first experimental evidence for complex cluster damage.

INTRODUCTION

DNA carries the genetic information inside the cells and represents a sensitive target of ionizing radiation. Ionizing radiations induce free radicals in DNA constituents and thereby produce various types of DNA lesions such as base damage, DNA single-strand breaks (SSBs), DNA double-strand breaks (DSBs), and DNA-protein crosslinks (1–3). Since ionizing radiation deposits energy along its track, the

spatial distribution of DNA lesions is not random. A region with two or more lesions within 10–20 bp is designated as clustered DNA damage (or locally multiply damaged sites) and is the hallmark of ionizing radiation (4,5). Chemical agents such as hydrogen peroxide also generate free radicals in DNA constituents and give rise to DNA lesions similar to those by ionizing radiation (6). However, hydrogen peroxide produces predominantly isolated damage and only rarely clustered DNA damage (7).

Among the isolated and clustered DNA damages produced by ionizing radiation, it is widely believed that clustered DNA damage is refractory to repair due to the influence of the vicinal lesion(s), unlike isolated DNA damage (8,9). Thus, clarifying the quantity and the complexity (i.e. the number of lesions per damage site) of clustered DNA damage is key to understanding the biological effect of ionizing radiation. This would be particularly important for high linear energy transfer (LET) radiations since the relative biological effectiveness (RBE) of ionizing radiation, as measured by cell killing, mutagenic effects and others, increases with increasing LET of up to 100–200 keV/μm (10,11). This increase is possibly related to the formation of complex clustered DNA damage.

DSB consisting of two vicinal SSBs (typically within 10–20 bp) located on opposing strands is the simplest clustered DNA damage. DSB is readily detected as DNA fragmentation or the induction of smaller DNA fragments in gel electrophoretic analysis. Simple clustered DNA damage consisting of vicinal base/base or base/SSB lesions (within 10–20 bp) in the opposing strands can also be detected by converting them into DSBs by the treatment with DNA glycosylases and/or apurinic/aprimidinic (AP) endonucleases. Accordingly, the formation of these simple clustered DNA damage has been well demonstrated experimentally in plas-

*To whom correspondence should be addressed. Tel: +81 82 424 7457; Fax: +81 82 424 7457; Email: ideh@hiroshima-u.ac.jp

Present addresses:

Toshiaki Nakano, Department of Quantum life Science, Quantum Beam Science Research Directorate, National Institutes of Quantum and Radiological Science and Technology, 8-1-7 Umemidai, Kizugawa-shi, Kyoto 619-0215, Japan.

Masataka Tsuda and Hiroshi Ide, Program of Mathematical and Life Sciences, Graduate School of Integrated Sciences for Life, Hiroshima University, Higashi-Hiroshima 739-8526, Japan.

mids (12), *Escherichia coli* (13), and mammalian cells (14–16). Monte Carlo simulations of the induction of clustered DNA damage predict that ionizing radiation produces complex clustered DNA damage consisting of more than three vicinal DNA lesions, together with simple clustered DNA damage that contains two vicinal DNA lesions (17,18). The complexity of clustered DNA damage is predicted to increase with increasing LET. However, whether ionizing radiation produces such complex clustered DNA damage remains to be demonstrated experimentally and is key to understanding the biological effect characteristic of ionizing radiation.

Here, we developed a novel method to visualize individual DNA lesions in DNA with atomic force microscopy (AFM) and analyzed clustered DNA damage. We irradiated plasmid DNA with sparsely ionizing radiation (X-rays) and densely ionizing radiation (Fe-ion beams) in aqueous solution. Irradiated DNA was treated with DNA glycosylases. The resulting AP sites were labeled with an aldehyde reactive probe (ARP) that has both the alkoxyamine for the reaction with the aldehyde group of DNA and the biotin moiety for the subsequent labeling (Figure 1) (19,20). Finally, the biotin moiety bound to DNA was tagged with streptavidin (53 kDa), and the resulting ARP-streptavidin complex was visualized with AFM to reveal the spatial distribution of damage along the DNA fiber.

MATERIALS AND METHODS

DNA model of clustered damage

DNA fragments (738 bp) containing one or two biotin-streptavidin tags as model clustered damage were prepared as described in the Supplementary Material.

Irradiation

X-rays were generated by an OHMIC OM-303M X-ray generator (70 kV, 3 mA, 0.2 mm Al filter). Fe-ion beams (500 MeV/amu) were generated by the Heavy Ion Medical Accelerator in Chiba (HIMAC) at the National Institute of Radiological Sciences. The dose rate and LET of X-rays were 3.7 Gy/min and 1.0 keV/ μm , respectively, and those of Fe-ion beams were 12 Gy/min and 200 keV/ μm (the plateau region of the Bragg curve), respectively. Plasmid pUC19 (4 μg) was irradiated with X-rays or Fe-ion beams (200 Gy) in 10 mM Tris-HCl (pH 7.5) and 1 mM EDTA (TE buffer, a total volume of 20 μl) at room temperature under aerobic conditions.

Fenton reactions

pUC19 DNA (4 μg) was incubated with 1 mM H_2O_2 and 0.3 mM $\text{Fe}(\text{NH}_4)_2(\text{SO}_4)_2/\text{EDTA}$ in 10 mM Tris-HCl (pH 7.5, a total volume of 20 μl) at 37°C for 2 h. After the reaction, DNA was separated from other reactants and purified by gel-filtration through Centri-Sep spin columns (Princeton Separations).

ARP and streptavidin labeling of DNA

After irradiation or the Fenton reaction, plasmid DNA (4 μg) was incubated simultaneously with *Escherichia coli*

endonuclease (Endo) III (20 units, New England Biolabs) and human 8-oxoguanine glycosylase (OGG1, 6 units, New England Biolabs) in 20 mM Tris-HCl (pH 8), 1 mM EDTA, 50 mM NaCl, 1 mM dithiothreitol (in a total volume of 30 μl) at 37°C for 1 h. After the reactions, the reaction buffer was changed to TE buffer using a Centri-Sep spin column. DNA (1.6 μg) was incubated with 5 mM ARP (Dojindo) in TE buffer (a total volume of 40 μl) at 37°C for 2 h. Free ARP was removed by a Centri-Sep spin column (twice) using phosphate buffered saline (pH 7.5, PBS) as an eluent. Finally, ARP-labeled DNA (0.25 μg) was incubated with streptavidin (tetramer, 8.5 μg , Wako Pure Chemical) in PBS (40 μl) at 37°C for 3 h. Free streptavidin was removed by a Chroma spin TE200 column (Mw cut off: $<1 \times 10^6$ for proteins and <70 bp for DNA, Clontech) using TE buffer as an eluent.

AFM imaging

One microliter of ARP-streptavidin-labeled DNA (2 ng/ μL) was mixed with 1 μl of 40 mM NiCl_2 . The sample (2 μl) was adsorbed onto a freshly cleaved mica plate (ϕ 1.5 mm, Research Institute of Biomolecule Metrology (RIBM) Co. Ltd) for 5 min at room temperature, and then the surface was gently washed twice using MilliQ water. AFM images were recorded using a high speed-scanning AFM system (Nano Live Vision, RIBM Co. Ltd) with an ultra-short cantilever (resonant frequency 1200 kHz, spring constant 0.15 N/m, tip radius <10 nm, NanoWorld USC-F1.2-k0.15). Scanning was performed using the tapping mode in MilliQ water. All images were recorded with an image acquisition speed of 1 frame/s. The DNA damage was quantified by counting the number of streptavidin-DNA complexes in the AFM images. The heights of streptavidin-DNA complexes were measured using IGOR Pro ver6.2 (WaveMetrics), and complexes with heights of 8–12 nm were considered as DNA damage. The heights of the DNA were 2–4 nm. The method for the AFM analysis of clustered DNA damage in plasmid DNA is given as a Supplementary protocol.

RESULTS

Resolution power of AFM for model clustered DNA damage

We first assessed the resolution power of our AFM system for clustered DNA damage using a DNA model for clustered damage. DNA fragments (738 bp) containing one or two biotin-streptavidin tags at defined damage sites were prepared as described in the Supplementary Material (Supplementary Figure S1). The two damage sites were 3 or 8 bases-apart on the same strand (Supplementary Figure S1C). In the AFM imaging of DNA, two streptavidin tags 3-bases-apart were observed as partially resolved peaks (Supplementary Figure S2 upper images). Among all the observed DNA fibers ($n = 216$), 62% of the damage sites showed the partial separation of streptavidin tags. Based on the different apparent heights of the ARP-streptavidin complex and DNA, 8–12 and 2–4 nm, respectively, they were readily distinguished from each other (Supplementary Figure S2 lower graphs). The separation of streptavidin tags

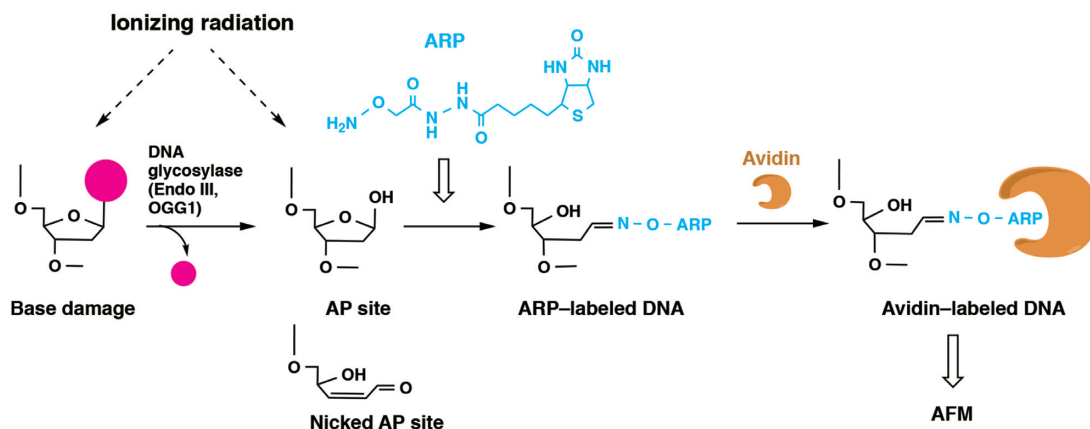


Figure 1. Principle of the visualization of DNA damage with AFM. Treatment of DNA with damaging agents (e.g. ionizing radiation) leads to the formation of base damage and AP sites. Base damage is converted to AP sites by treatment with DNA glycosylases that excise oxidized pyrimidine bases (Endo III) and purine bases (OGG1) from DNA. The aldehyde group in the AP site resulting from a glycosylase reaction or direct radiation is labeled with biotin-containing ARP, which is then bound by streptavidin (tetramer, 53 kDa). Finally, the ARP-streptavidin complex is visualized with AFM to reveal the spatial distribution of damages in the DNA fiber. The nicked AP site containing aldehyde can also be labeled with ARP and visualized with AFM in a similar manner.

was 58% for the DNA model with damaged sites 8-base-apart. Thus, the resolution was $\sim 60\%$ for either damage sites models (3 or 8 bases-apart). Accordingly, the resolution power of AFM was reasonably good for observing closely separated DNA lesions in radiation-induced clustered damage. In the DNA locations where streptavidin tags were not separately observed, their separate observation by AFM might have been precluded by their overlap.

In the present AFM imaging, the apparent diameter size of the streptavidin tag (a tetramer) was $\sim 10\text{--}15$ nm, corresponding to the apparent DNA length of 29–44 bp (on average = 37 bp). Accordingly, two lesions separated by $>29\text{--}44$ bp were completely resolved in the present study, whereas those with an inter-lesion distance $<29\text{--}44$ bp were partially resolved. Also, the intrinsic inter-lesion distance of the latter lesions could not be accurately determined by AFM imaging due to the mutual steric exclusion of adjacent streptavidin tags. Thus, in the present study, we tentatively used a slightly modified definition of clustered damage. Although the conventional definition is a site containing two or more lesions within 10–20 bp, we modified the definition to site containing two or more lesions within 37 bp. In addition, we consider that in AFM imaging, two or more streptavidin tags that contact each other represent clustered DNA damage, whereas those with baseline separation represent isolated DNA damage.

X-rays produce simple clustered damage

pUC19 plasmid DNA (2,686 bp) was irradiated with 200 Gy of X-rays (LET = 1 keV/ μm) in TE buffer under aerobic conditions. The irradiated plasmid DNA was treated with saturating amounts of Endo III and OGG1 that excise oxidized pyrimidine and purine bases, respectively (21–24). While Endo III has concerted glycosylase and AP lyase activities, OGG1 possesses weak AP lyase activity and inefficiently incises AP sites (25,26). The resulting AP sites, a mixture of intact and nicked forms, were labeled with ARP followed by streptavidin (Figure 1) and observed with AFM.

The intact and nicked forms of AP sites are also formed directly by ionizing radiation (prompt AP sites). Such prompt AP sites cannot be distinguished from those produced by Endo III and OGG1 treatments. Accordingly, AP sites were tentatively classified into base damage in the present study.

AFM analysis revealed that untreated control plasmid ($n = 607$) contained isolated damage (8.6%) and clustered damage (1.6%) (Figure 2A). These lesions were produced during the purification of plasmid DNA. Irradiation of plasmid with X-rays resulted in 48.3% undamaged plasmid (Figure 2A). This value corresponds to 0.73 lesions per plasmid on average, assuming a Poisson distribution for radiation damage upon irradiation. Therefore, in the present study, the average damage rate was less than one per plasmid for X-rays. With X-ray-irradiated plasmids ($n = 619$), the percentages of plasmids containing isolated and clustered damage were 43.3% and 8.4%, respectively (Figure 2A). In AFM imaging, up to 4 isolated lesions were observed in a single plasmid molecule (Figure 3A). However, the proportions of plasmids containing two, three and four isolated lesions were significantly lower (6.0%, 1.6% and 0.2%, respectively) than that with one isolated lesion (35.5%) (Figure 2B). This indicates that the formation of multiple isolated lesions in one plasmid molecule is a rare event under the present conditions. This was also true for Fe-ion beams and Fenton's reagent (see sections below). The types of clustered damage generated by X-rays were DSB (3.55%), two vicinal damaged bases (B/B, 1.93%), DSB with a flanking base damage (DSB/B, 2.42%), and DSB with a flanking base damage on both sides of the DSB (B/DSB/B, 0.323%) (Figure 2C). We adopted the following notation convention for clustered damage throughout the text: the components of clustered damage (damaged base (B) and DSB) are separated by a slash (/), and the order of the components indicates their relative position (Supplementary Figure S3). AFM images of typical clustered damage by X-rays are shown in Figure 3B. Although minor, X-rays also generated two separated clustered damage sites in one plasmid molecule that contained DSB and two vicinal damaged

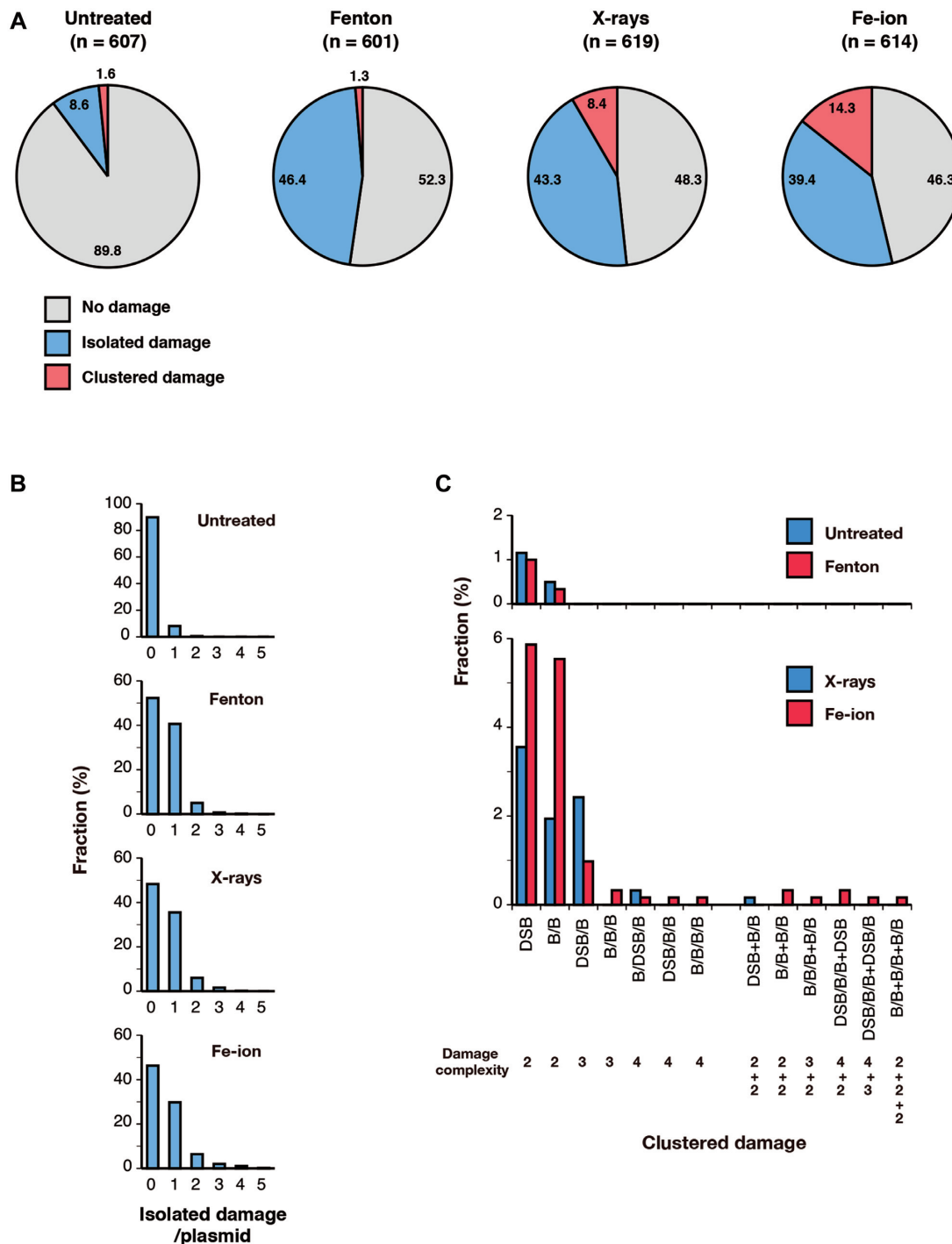


Figure 2. Isolated and clustered DNA damage induced by the Fenton reaction, X-rays, and Fe-ion beams. (A) Fractions of plasmids containing no damage (white), isolated damage (blue), and clustered damage (red). pUC19 plasmid DNA was treated by the Fenton reaction or irradiated with 200 Gy of X-rays (1 keV/μm) or Fe-ion beams (200 keV/μm). DNA damage was visualized and quantified by AFM as shown in Figure 1. Percentages of the respective damages are shown on the graphs. 'n' indicates the number of plasmids analyzed with AFM. (B) Percentage (%) of plasmids containing 0, 1, 2, 3, 4 and 5 isolated lesions in one plasmid molecule. Data are derived from samples shown in panel A. (C) Spectra of clustered damage for untreated plasmid and plasmid treated by the Fenton reaction (upper graphs) and plasmid irradiated with X-rays or Fe-ion beams (lower graphs). Percentages (%) of plasmids containing the indicated types of clustered damage are plotted. Data are derived from samples shown in panel A. The types of clustered damage are DSB, two vicinal damaged bases (B/B), DSB with a flanking base damage (DSB/B), three vicinal damaged bases (B/B/B), DSB with a flanking base damage on both sides of the DSB (B/DSB/B) and four vicinal damaged bases (B/B/B/B). The types of separated multiple clustered damage sites in one plasmid molecule are a combination of DSB and two vicinal damaged bases (DSB+B/B), a combination of two vicinal damaged bases (B/B+B/B), a combination of three and two vicinal damaged bases (B/B/B+B/B), and three sets of two vicinal damaged bases (B/B+B/B+B/B). For the notation of clustered damage, see also Supplementary Figure S3. The damage complexity indicates the number of lesions per clustered DNA damage site. AP sites were classified into base damage.

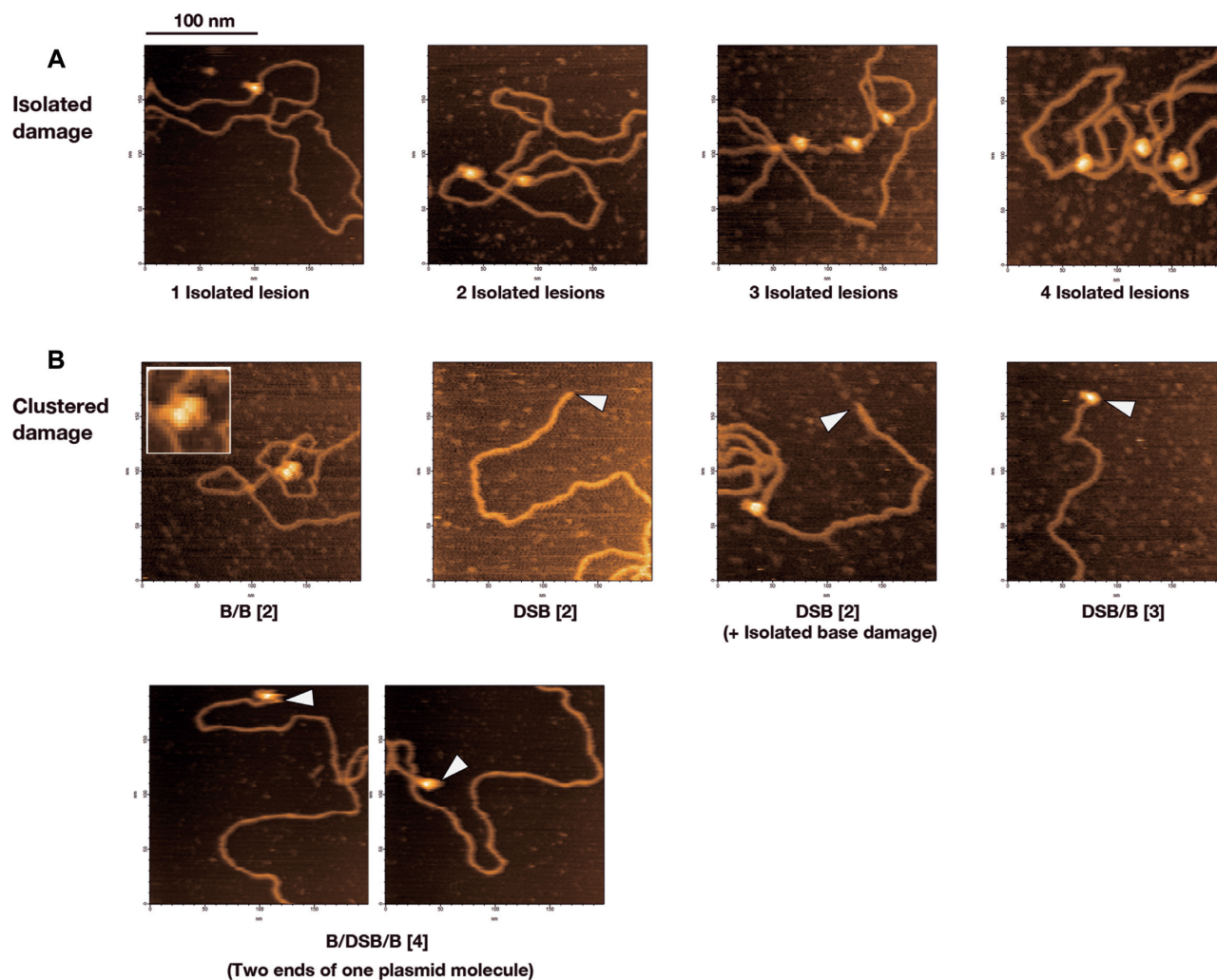


Figure 3. AFM imaging of DNA damage in plasmids irradiated with X-rays. (A) Plasmids containing 1, 2, 3 and 4 isolated lesions per plasmid molecule, (B) Plasmids containing clustered damage: two vicinal damaged bases (B/B) (Inset: enlarged view of B/B), DSB, DSB with a flanking base damage (DSB/B) and DSB with a flanking base damage on both sides of the DSB (B/DSB/B). The arrowhead indicates the DSB end of the plasmid. The number in brackets next to the type of damage indicates the damage complexity.

bases (DSB+B/B, 0.161%, Figure 2C), where the plus sign (+) indicates the combination of clustered damages (Supplementary Figure S3).

With X-rays, the complexity of clustered damage (i.e. the number of lesions per damage site) was two (DSB and B/B, 5.48%), three (DSB/B, 2.42%), four (B/DSB/B, 0.323%), and two + two (DSB+B/B, 0.161%) (Figure 2C), indicating that sparsely ionizing X-rays predominantly produce relatively simple clustered damages with a complexity of two and three. The formation of DSB with a flanking base damage (DSB/B) was previously demonstrated in plasmid DNA by triplex-forming oligonucleotide-targeted ^{125}I decay (27,28).

Fe-ion beams produce two types of complex clustered damage

pUC19 plasmid DNA was irradiated with 200 Gy of Fe-ion beams (LET = 200 keV/ μm), labeled with ARP and streptavidin, and observed with AFM as described for X-rays. Irradiation of plasmid DNA resulted in 46.3% undamaged

plasmid (Figure 2A). This value corresponded to 0.77 lesions per plasmid on average, assuming a Poisson distribution, indicating that the average damaging event was less than one per plasmid for Fe-ion beams. Fe-ion beams produced isolated and clustered damage. Fractions of the plasmid ($n = 614$) containing isolated and clustered damages were 39.4% and 14.3%, respectively (Figure 2A), showing an increase in the yield of clustered damage relative to X-rays. Fe-ion beams produced up to five isolated lesions in a single plasmid molecule, but plasmids containing 2, 3, 4 and 5 isolated lesions (6.4%, 2.0%, 1.1% and 0.2%, respectively) were underrepresented relative to those containing one isolated lesion (29.8%) (Figure 2B), indicating that the formation of multiple isolated lesions in one plasmid molecule is rare event. Interestingly, the spectra of clustered damages associated with Fe-ion beams was dramatically different from that with X-rays. Fe-ion beams generated complex clustered damages including those with three vicinal damaged bases (B/B/B), four vicinal damaged bases (B/B/B/B) and DSB with two flanking base damages on one side of

the DSB (DSB/B/B) (Figure 2C and Supplementary Figure S3), which were not observed with X-rays, together with simple clustered damages (DSB, B/B and DSB/B), which were observed with X-rays. AFM images of typical clustered damage by Fe-ion beams are shown in Figure 4A and C. As for X-rays, the highest complexity of clustered damage for Fe-ion beams was four (B/DSB/B, DSB/B/B and B/B/B/B). The plasmid fraction with the highest complexity was 0.486% for Fe-ion beams and 0.324% for X-rays, suggesting a slight preferential formation of clustered damage with the highest complexity for Fe-ion beams.

Notably, Fe-ion beams generated multiple (i.e. two or three) clustered damage sites in one plasmid molecule at significant levels. These include plasmids containing a combination of two vicinal damaged bases (B/B+B/B), a combination of three and two vicinal damaged bases (B/B/B+B/B), and three sets of two vicinal damaged bases (B/B+B/B+B/B) (Figure 2C). AFM images of typical two clustered damage sites by Fe-ion beams are shown in Figure 4B. In addition, plasmid fragments containing two complex DSB ends (DSB/B/B+DSB, ca 870 bp, and DSB/B/B+DSB/B, ca 1100 bp) were also observed with Fe-ion beams (Figures 2C, 4B and Supplementary Figure S3). The plasmid fraction containing multiple clustered damage sites in one plasmid molecule was 1.136% for Fe-ion beams and 0.161% for X-rays. Thus, the formation of multiple clustered damage sites in one plasmid molecule is the hallmark of densely ionizing Fe-ion beams and represents an event associated with a single densely ionizing track of Fe-ion beams as discussed below (see Discussion).

Fenton reactions produce exclusively isolated lesions

To compare the spatial damage distribution, plasmid DNA was treated with Fenton's reagent and the resulting DNA damage was analyzed by AFM. Although Fenton reactions cause DNA oxidation and give rise to base and sugar lesions similar to those produced by ionizing radiation, the spatial distribution of DNA lesions formed by Fenton reactions is random and isolated lesions are formed exclusively (6,7). In the Fenton reaction-treated plasmid sample ($n = 601$), the plasmid fraction containing no damage was 52.3% (Figure 2A), a percentage comparable to those for X-rays and Fe-ion beams (48.3% and 46.3%). However, the percentage of the plasmid with clustered damage (1.3%) was virtually similar between Fenton reactions and untreated plasmid (1.6%). Thus, Fenton reactions produced exclusively isolated lesions. Fenton reactions produced up to four isolated lesions per plasmid, but plasmids containing two, three and four isolated lesions (5.0%, 0.7% and 0.2%, respectively) were minor relative to plasmids containing one isolated lesion (40.6%) (Figure 2B), indicating that the formation of multiple isolated lesions in a single plasmid molecule is a rare event. Thus, Fenton reactions, X-rays, and Fe-ion beams are similar with respect to the multiplicity of isolated lesions per plasmid (Figure 2B). This similarity also indicates that as with Fenton reactions, the multiple isolated lesions observed with X-rays and Fe-ion beams were produced through uncorrelated multiple hits (through a direct or indirect mechanism) that occurred with frequencies much lower than for a single hit.

It should be noted that after damage induction by X-rays, Fe-ion beams, and the Fenton reaction, all DNA samples were treated and processed in the same manner in the present study. The absence of clustered DNA damage formation by the Fenton reaction indicates that clustered DNA damage observed for irradiated DNA (Figure 3 for X-rays and Figure 4 for Fe-ion beams) is not an artifact of sample preparation or AFM observation. This also rules out the possibility of accidental overlapping of DNA lesions that yield false-positive results regarding the formation of clustered DNA damage.

DISCUSSION

In this study, we established a novel method to directly observe the spatial distribution of DNA lesions in DNA fibers. DNA lesions in irradiated plasmid DNA were tagged with ARP/streptavidin and observed with AFM. Our method allows not only to estimate the frequency but to analyze the complexity of clustered DNA damage. In addition, while not easily, it can in principle be applied to the damage analysis of chromosomal DNA isolated from irradiated cells. Knowing that more complex are the clustered damages, less repaired and more deleterious they are, it is important to determine those parameters when using high LET radiations for the therapy of cancer (hadrontherapy) (10,11). Furthermore, the data obtained in the present study demonstrate that clustered DNA damage of high complexity can be produced. This gives weight to the numerous *in vitro/in vivo* repair studies using synthetic clustered DNA damage composed of several lesions within a few helical turns (8,9). In addition, there have been a number of reports on the production of clustered DNA damage by agents other than ionizing radiation, like UVA (9). Most of these studies are subject of controversy. The present method should help in clarifying the situation.

In previous studies, AFM has been used exclusively to measure the size distribution of DNA fragments after *in vitro* irradiation of plasmids (reviewed in (29)). The results of these studies show that high LET radiations produce short DNA fragments more efficiently than low LET radiations, indicating the dense clustering of DSBs with high LET radiations. The minimum size of the short DNA fragments that could be detected with AFM was 150 bp (50 nm)–300 bp (100 nm) (30–32). Thus, the resolution power for clustered DSBs was 150–300 bp in the previous AFM studies. Notably, the resolution power for clustered DNA lesions has been significantly improved to be ~37 bp in the present AFM method. Gel electrophoretic analysis of macromolecular DNA has also been used to analyze clustered DNA damage (33,34). Prompt and repair enzyme-induced DSBs reduce the size of macromolecular DNA. The average number of such lesions per unit length of DNA can be calculated from the size distribution of DNA. However, in such analysis, short DNA fragments resulting from clustered DSBs may not be detectable due to sensitivity limitations. Also, the size analysis of DNA by gel electrophoretic method cannot distinguish between complex clustered DNA damage containing more than three vicinal lesions and simple clustered DNA damage containing two vicinal lesions (see Introduction). This problem has been

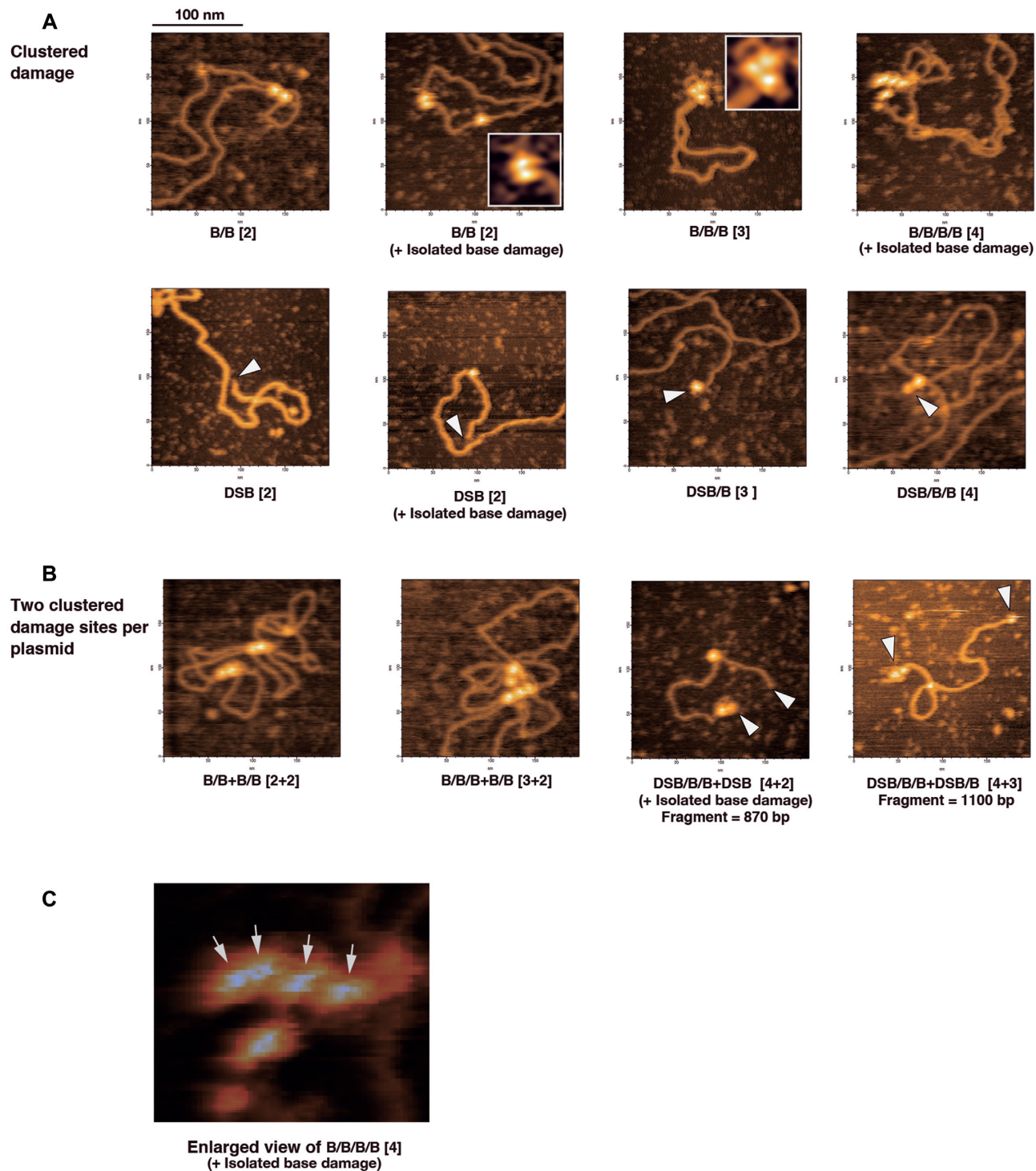


Figure 4. AFM imaging of DNA damage in plasmids irradiated with Fe-ion beams. (A) Plasmids containing clustered damage: two vicinal damaged bases (B/B, Inset: enlarged view of B/B), three vicinal damaged bases (B/B/B, Inset: enlarged view of B/B/B), four vicinal damaged bases (B/B/B/B, for enlarged view see panel C), DSB, DSB with a flanking base damage (DSB/B), DSB with two flanking base damages on one side of the DSB (DSB/B/B), (B) Plasmids containing two clustered damage sites: a combination of two vicinal damaged bases (B/B+B/B), a combination of three and two vicinal damaged bases (B/B/B+B/B), fragments of plasmid containing two complex DSB ends (DSB/B/B+DSB, ca 870 bp, and DSB/B/B+DSB/B, ca 1100 bp). In panels A and B, the arrowhead indicates the DSB end of the plasmid. The number in brackets next to the type of damage indicates the damage complexity. (C) Enlarged views of the clustered damage containing four vicinal damaged bases (B/B/B/B) shown in (A), The arrows indicate individual lesions.

overcome by directly observing DNA lesions with AFM after labeling with ARP/streptavidin in the present study.

The present study showed that densely ionizing Fe-ion beams (high LET radiation, 200 keV/ μm) induced two types of DNA damage clustering. One was the formation of complex clustered DNA damage containing two to four lesions (Figures 2C and 4A). The other was the formation of multiple (i.e. two or three) clustered damage sites in a plasmid molecule (Figures 2C and 4B).

Regarding the first type of damage clustering, Monte Carlo simulations of the radiation track have indicated the LET-dependent formation of complex clustered DNA damage. First, the fraction of complex DSBs with at least one vicinal lesion (including base damage) is about 30% at low LET, whereas it is 90% at high LET (17). Second, X-rays (LET = 4.6 keV/ μm) produce clustered damages containing 1, 2, 3, 4 and 5 lesions (strand breaks and base damages) with an approximate ratio of 55:13:5:2.2:1, whereas the ratio is 3.9:2.7:2:1.4:1 for Fe-ion beams (LET = 165 keV/ μm) (18). The present results provide the first experimental evidence of the formation of complex clustered DNA damage containing up to four lesions. The present estimation of the number of lesions in clustered damage represents a lower limit since some of the radiation-induced DNA lesions are not labeled with ARP by the present method due to the absence of the aldehyde group or the impairment of Endo III/OGG1 glycosylases for very closely spaced lesions, and therefore cannot be detected. Meanwhile, the data relative to X-rays (low LET), Fe-ion beams (high LET) and Fenton reactions are in good agreement with what predicted (X-rays and Fe-ion beams) and known (Fenton reaction products). Therefore, the underestimation of the values for the clusters (i.e. yields and complexity) may not be so severe with the present method. Here we show that DNA lesions in clustered damage are close to each other (<37 bp), although their exact spacing was not obtained due to the mutual steric exclusion of streptavidin tags. If DNA lesions are very close to each other, they could be refractory to repair due to the disrupting influence of the vicinal lesion(s) on repair enzymes/proteins. The lack of repair would cause increased levels of cell death and/or mutations. Indeed, high RBE values are characteristic of high LET radiations such as Fe-ion beams (10,11).

The second type of DNA damage clustering induced by Fe-ion beams is the formation of multiple clustered damage sites in a single plasmid molecule. This was rarely observed for X-rays (Figure 2C). The separation of two clustered damage sites in the irradiated plasmid was estimated to range from 200 to 1100 bp based on the distribution of clustered damage sites (Figure 4B). There are two possible mechanisms for the formation of these lesions. In the first mechanism, two clustered damage sites are associated with the hit of a single track of Fe-ion beams. Thus, their formation is a correlated event. In the second mechanism, they are produced by the hit of two or more separate tracks of Fe-ion beams, and their formation is due to independent events. If the second mechanism was operating, X-rays should also have generated multiple clustered damage sites with low damage complexity such as B/B+B/B and DSB+B/B in a plasmid molecule. However, such clustered damage sites were rarely observed in X-ray-irradiated plas-

mids (Figure 2C), eliminating the possibility of the second mechanism. In keeping with this notion, the number of Fe-ion particles that traverse pUC19 DNA is estimated to be 0.011 per plasmid molecule at 200 Gy according to the flux of the beam used in this study (data not shown). Notably, the number of DNA lesions induced by Fe-ion beams was much greater (0.77 per plasmid), since the Coulomb attraction of electrons by the charged particle caused ionization of DNA and water molecules that were away from the track. If two clustered damage sites with a spacing of 200–1100 bp are formed by Fe-ion beams and subjected to repair simultaneously in cells, some of them could be concurrently converted into two DSBs, and hence lead to chromosome aberrations such as deletions and chromosome rearrangements, which are characteristic of high LET radiations (35–37).

According to Monte Carlo simulations, multiple correlated DSBs (i.e. clustered DSBs) are formed in folded chromatin fibers when cells are irradiated by ionizing radiation (38,39). Consistent with this, LET-dependent formation of short DNA fragments probably associated with correlated proximal DSBs was experimentally observed in irradiated cells (39–41). It was also shown that high LET irradiations generate a significantly larger fraction of short DNA fragments than low LET irradiations when plasmid DNA is very heavily irradiated (typically 1–6 kGy) (29–32). These data are mechanistically consistent with the formation of correlated clustered damage in a plasmid molecule in the present study.

In contrast to Fe-ion beams, sparsely ionizing X-rays (low LET radiation, 1 keV/ μm) mainly produced clustered damage with relatively low damage complexity as shown in Figure 2C. Also, X-rays rarely induce correlated clustered damage sites in plasmids. Thus, X-rays intrinsically produce relatively simple clustered damages. These data are consistent with the lower RBE relative to Fe-ion beams exhibited by X-rays.

DSBs are the simplest clustered damage induced by ionizing radiation. DSBs can be indirectly detected by immunofluorescence microscopy (IFM) that visualizes proteins involved in the repair of DSBs such as phosphorylated H2AX (γH2AX) and p53-binding protein 1 (53BP1) (42). In addition, the use of high-resolution fluorescence microscopes enabled DSB observation with a higher spatial resolution (43,44). IFM detection of DSBs provided insights into the subnuclear distributions of DSBs. Recently, proteins involved in DSB repair were immuno-labeled with gold-labeled antibodies and detected by transmission electron microscope (TEM) with an even higher resolution than that achieved with IFM (45,46). The results showed that clustering of DSBs generated by high LET radiations depended on the chromatin packing density, providing insights into DSB distributions in different chromatin contexts. Indirect detection of DSBs by IFM or TEM showed that high LET heavy ions induced multiple DSBs in close proximity along the particle track. However, how DNA lesions are distributed along the DNA fiber cannot be shown with these techniques. Also, it is not clear whether DNA lesions are clustered within a few helical turns since individual DNA fibers were not visualized. The present method of damage detection could be applied to chromosomal DNA isolated from irradiated cells, then the question relative to

the DNA lesions distribution along the DNA fiber could be answered. This would allow identifying what type of clustered DNA damage (i.e. complex clustered damage) is refractory to repair and is causing cell death and mutations.

SUPPLEMENTARY DATA

Supplementary Data are available at NAR Online.

ACKNOWLEDGEMENTS

We thank the members of the Ide lab for their helpful discussions.

FUNDING

KAKENHI grant from the Ministry of Education, Culture, Sports, Science and Technology [16H01642 to H.I.]; Japan Society for Promotion of Science [18H03374 to H.I.]. Funding for open access charge: KAKENHI grant from Japan Society for Promotion of Science [18H03374].

Conflict of interest statement. None declared.

REFERENCES

- Pouget, J.P., Frelon, S., Ravanat, J.L., Testard, I., Odin, F. and Cadet, J. (2002) Formation of modified DNA bases in cells exposed either to gamma radiation or to high-LET particles. *Radiat. Res.*, **157**, 589–595.
- Dizdaroglu, M. and Jaruga, P. (2012) Mechanisms of free radical-induced damage to DNA. *Free Radic. Res.*, **46**, 382–419.
- Nakano, T., Xu, X., Salem, A.M.H., Shoukamy, M.I. and Ide, H. (2017) Radiation-induced DNA-protein cross-links: Mechanisms and biological significance. *Free Radic. Biol. Med.*, **107**, 136–145.
- Ward, J.F. (1994) The complexity of DNA damage: relevance to biological consequences. *Int. J. Radiat. Biol.*, **66**, 427–432.
- Goodhead, D.T. (1994) Initial events in the cellular effects of ionizing radiations: clustered damage in DNA. *Int. J. Radiat. Biol.*, **65**, 7–17.
- Henle, E.S. and Linn, S. (1997) Formation, prevention, and repair of DNA damage by iron hydrogen peroxide. *J. Biol. Chem.*, **272**, 19095–19098.
- Ward, J.F., Blakely, W.F. and Joner, E.I. (1985) Mammalian cells are not killed by DNA single-strand breaks caused by hydroxyl radicals from hydrogen-peroxide. *Radiat. Res.*, **103**, 383–392.
- Eccles, L.J., O'Neill, P. and Lomax, M.E. (2011) Delayed repair of radiation induced clustered DNA damage: friend or foe? *Mutat. Res.*, **711**, 134–141.
- Sage, E. and Shikazono, N. (2017) Radiation-induced clustered DNA lesions: Repair and mutagenesis. *Free Rad. Biol. Med.*, **107**, 125–135.
- Durante, M. (2014) New challenges in high-energy particle radiobiology. *Br. J. Radiol.*, **87**, 20130626.
- Held, K.D., Kawamura, H., Kaminuma, T., Paz, A.E.S., Yoshida, Y., Liu, Q., Willers, H. and Takahashi, A. (2016) Effects of charged particles on human tumor cells. *Front. Oncol.*, **6**, 23.
- Prise, K.M., Pullar, C.H.L. and Michael, B.D. (1999) A study of endonuclease III-sensitive sites in irradiated DNA: detection of alpha-particle-induced oxidative damage. *Carcinogenesis*, **20**, 905–909.
- Blaisdell, J.O. and Wallace, S.S. (2001) Abortive base-excision repair of radiation-induced clustered DNA lesions in *Escherichia coli*. *Proc. Natl. Acad. Sci. U.S.A.*, **98**, 7426–7430.
- Sutherland, B.M., Bennett, P.V., Sidorkina, O. and Laval, J. (2000) Clustered DNA damages induced in isolated DNA and in human cells by low doses of ionizing radiation. *Proc. Natl. Acad. Sci. U.S.A.*, **97**, 103–108.
- Sutherland, B.M., Bennett, P.V., Sutherland, J.C. and Laval, J. (2002) Clustered DNA damages induced by X rays in human cells. *Radiat. Res.*, **157**, 611–616.
- Gulston, M., Fulford, J., Jenner, T., de Lara, C. and O'Neill, P. (2002) Clustered DNA damage induced by radiation in human fibroblasts (HF19), hamster (V79-4) cells and plasmid DNA is revealed as Fpg and Nth sensitive sites. *Nucleic Acids Res.*, **30**, 3464–3472.
- Nikjoo, H., O'Neill, P., Wilson, W.E. and Goodhead, D.T. (2001) Computational approach for determining the spectrum of DNA damage induced by ionizing radiation. *Radiat. Res.*, **156**, 577–583.
- Watanabe, R., Rahmanian, S. and Nikjoo, H. (2015) Spectrum of radiation-induced clustered non-DSB damage - a Monte Carlo track structure modeling and calculations. *Radiat. Res.*, **183**, 525–540.
- Ide, H., Akamatsu, K., Kimura, Y., Michiue, K., Makino, K., Asaeda, A., Takamori, Y. and Kubo, K. (1993) Synthesis and damage specificity of a novel probe for the detection of abasic sites in DNA. *Biochemistry*, **32**, 8276–8283.
- Ali, M.M., Kurisu, S., Yoshioka, Y., Terato, H., Ohshima, Y., Kubo, K. and Ide, H. (2004) Detection of endonuclease III- and 8-oxoguanine glycosylase-sensitive base modifications in gamma-irradiated DNA and cells by the aldehyde reactive probe (ARP) assay. *J. Radiat. Res.*, **45**, 229–237.
- Dizdaroglu, M., Laval, J. and Boiteux, S. (1993) Substrate specificity of the *Escherichia coli* endonuclease-III: Excision of thymine- and cytosine-derived lesions in DNA produced by radiation-generated free radicals. *Biochemistry*, **32**, 12105–12111.
- Katafuchi, A., Nakano, T., Masaoka, A., Terato, H., Iwai, S., Hanaoka, F. and Ide, H. (2004) Differential specificity of human and *Escherichia coli* endonuclease III and VIII homologues for oxidative base lesions. *J. Biol. Chem.*, **279**, 14464–14471.
- Dherin, C., Radicella, J.P., Dizdaroglu, M. and Boiteux, S. (1999) Excision of oxidatively damaged DNA bases by the human alpha-hOgg1 protein and the polymorphic alpha-hOgg1(Ser326Cys) protein which is frequently found in human populations. *Nucleic Acids Res.*, **27**, 4001–4007.
- Asagoshi, K., Yamada, T., Terato, H., Ohshima, Y., Monden, Y., Arai, T., Nishimura, S., Aburatani, H., Lindahl, T. and Ide, H. (2000) Distinct repair activities of human 7,8-dihydro-8-oxoguanine DNA glycosylase and formamidopyrimidine DNA glycosylase for formamidopyrimidine and 7,8-dihydro-8-oxoguanine. *J. Biol. Chem.*, **275**, 4956–4964.
- Hill, J.W., Hazra, T.K., Izumi, T. and Mitra, S. (2001) Stimulation of human 8-oxoguanine-DNA glycosylase by AP-endonuclease: potential coordination of the initial steps in base excision repair. *Nucleic Acids Res.*, **29**, 430–438.
- Vidal, A.E., Hickson, I.D., Boiteux, S. and Radicella, J.P. (2001) Mechanism of stimulation of the DNA glycosylase activity of hOGG1 by the major human AP endonuclease: bypass of the AP lyase activity step. *Nucleic Acids Res.*, **29**, 1285–1292.
- Datta, K., Neumann, R.D. and Winters, T.A. (2005) Characterization of complex apurinic/apyrimidinic-site clustering associated with an authentic site-specific radiation-induced DNA double-strand break. *Proc. Natl. Acad. Sci. U.S.A.*, **102**, 10569–10574.
- Datta, K., Jaruga, P., Dizdaroglu, M., Neumann, R.D. and Winters, T.A. (2006) Molecular analysis of base damage clustering associated with a site-specific radiation-induced DNA double-strand break. *Radiat. Res.*, **166**, 767–781.
- Pang, D., Thierry, A.R. and Dritschilo, A. (2015) DNA studies using atomic force microscopy: capabilities for measurement of short DNA fragments. *Front. Mol. Biosci.*, **2**, 1.
- Elsasser, T., Brons, S., Psonka, K., Scholz, M., Gudowska-Nowak, E. and Taucher-Scholz, G. (2008) Biophysical modeling of fragment length distributions of DNA plasmids after X and heavy-ion irradiation analyzed by atomic force microscopy. *Radiat. Res.*, **169**, 649–659.
- Psonka, A., Antoniczyk, K., Elsasser, T., Gudowska-Nowak, E. and Taucher-Scholz, G. (2009) Distribution of double-strand breaks induced by ionizing radiation at the level of single DNA molecules examined by atomic force microscopy. *Radiat. Res.*, **172**, 288–295.
- Pang, D., Chasovskikh, S., Rodgers, J.E. and Dritschilo, A. (2016) Short DNA fragments are a hallmark of heavy charged-particle irradiation and may underlie their greater therapeutic efficacy. *Front. Oncol.*, **6**, 130.
- Sutherland, B.M., Georgakilas, A.G., Bennett, P.V., Laval, J. and Sutherland, J.C. (2003) Quantifying clustered DNA damage induction and repair by gel electrophoresis, electronic imaging and number average length analysis. *Mutat. Res.*, **531**, 93–107.

34. Sutherland, B.M., Bennett, P.V., Georgakilas, A.G. and Sutherland, J.C. (2003) Evaluation of number average length analysis in quantifying double strand breaks in genomic DNAs. *Biochemistry*, **42**, 3375–3384.
35. Singleton, B.K., Griffin, C.S. and Thacker, J. (2002) Clustered DNA damage leads to complex genetic changes in irradiated human cells. *Cancer Res.*, **62**, 6263–6269.
36. Hada, M., Cucinotta, F.A., Gonda, S.R. and Wu, H.L. (2007) mBAND analysis of chromosomal aberrations in human epithelial cells exposed to low- and high-LET radiation. *Radiat. Res.*, **168**, 98–105.
37. Asaithamby, A., Hu, B.R. and Chen, D.J. (2011) Unrepaired clustered DNA lesions induce chromosome breakage in human cells. *Proc. Natl. Acad. Sci. U.S.A.*, **108**, 8293–8298.
38. Holley, W.R. and Chatterjee, A. (1996) Clusters of DNA damage induced by ionizing radiation: Formation of short DNA fragments. 1. Theoretical modeling. *Radiat. Res.*, **145**, 188–199.
39. Friedland, W., Dingfelder, M., Kundrat, P. and Jacob, P. (2011) Track structures, DNA targets and radiation effects in the biophysical Monte Carlo simulation code PARTRAC. *Mutat. Res.*, **711**, 28–40.
40. Rydberg, B. (1996) Clusters of DNA damage induced by ionizing radiation: formation of short DNA fragments. 2. Experimental detection. *Radiat. Res.*, **145**, 200–209.
41. Lobrich, M., Cooper, P.K. and Rydberg, B. (1996) Non-random distribution of DNA double-strand breaks induced by particle irradiation. *Int. J. Radiat. Biol.*, **70**, 493–503.
42. Bekker-Jensen, S. and Mailand, N. (2010) Assembly and function of DNA double-strand break repair foci in mammalian cells. *DNA Repair (Amst.)*, **9**, 1219–1228.
43. Reindl, J., Girst, S., Walsh, D.W.M., Greubel, C., Schwarz, B., Siebenwirth, C., Drexler, G.A., Friedl, A.A. and Dollinger, G. (2017) Chromatin organization revealed by nanostructure of irradiation induced gamma H2AX, 53BP1 and Rad51 foci. *Sci. Rep.*, **7**, 40616.
44. Reid, D.A., Keegan, S., Leo-Macias, A., Watanabe, G., Strande, N.T., Chang, H.H., Oksuz, B.A., Fenyó, D., Lieber, M.R., Ramsden, D.A. et al. (2015) Organization and dynamics of the nonhomologous end-joining machinery during DNA double-strand break repair. *Proc. Natl. Acad. Sci. U.S.A.*, **112**, E2575–E2584.
45. Rube, C.E., Lorat, Y., Schuler, N., Schanz, S., Wennemuth, G. and Rube, C. (2011) DNA repair in the context of chromatin: New molecular insights by the nanoscale detection of DNA repair complexes using transmission electron microscopy. *DNA Repair (Amst.)*, **10**, 427–437.
46. Lorat, Y., Brunner, C.U., Schanz, S., Jakob, B., Taucher-Scholz, G. and Rube, C.E. (2015) Nanoscale analysis of clustered DNA damage after high-LET irradiation by quantitative electron microscopy - the heavy burden to repair. *DNA Repair (Amst.)*, **28**, 93–106.